APL Materials

Direct observation of bi-alkali antimonide photocathodes growth via *in operando* x-ray diffraction studies

Cite as: APL Mater. **2**, 121101 (2014); https://doi.org/10.1063/1.4902544
Submitted: 24 September 2014 • Accepted: 13 November 2014 • Published Online: 01 December 2014

M. Ruiz-Osés, S. Schubert, K. Attenkofer, et al.

Direct observation of bi-alkali antimonide photocathodes growth via *in operando* x-ray diffraction studies

M. Ruiz-Osés,[1,a] S. Schubert,[2,3] K. Attenkofer,[3] I. Ben-Zvi,[1] X. Liang,[1] E. Muller,[1] H. Padmore,[4] T. Rao,[3] T. Vecchione,[4,b] J. Wong,[4] J. Xie,[5] and J. Smedley[3,c]

[1]*Stony Brook University, Stony Brook, New York 11794, USA*
[2]*Helmholtz-Zentrum Berlin, Albert-Einstein Str. 15, 12489 Berlin, Germany*
[3]*Brookhaven National Laboratory, Upton, New York 11973, USA*
[4]*Lawrence Berkeley National Laboratory, Berkeley, California 94720, USA*
[5]*Argonne National Laboratory, Lemont, Illinois 60439, USA*

(Received 24 September 2014; accepted 13 November 2014; published 1 December 2014)

Alkali antimonides have a long history as visible-light-sensitive photocathodes. This work focuses on the process of fabrication of the bi-alkali photocathodes, K_2CsSb. *In-situ* synchrotron x-ray diffraction and photoresponse measurements were used to monitor phase evolution during sequential photocathode growth mode on Si(100) substrates. The amorphous-to-crystalline transition for the initial antimony layer was observed at a film thickness of 40 Å. The antimony crystalline structure dissolved upon potassium deposition, eventually recrystallizing upon further deposition into K-Sb crystalline modifications. This transition, as well as the conversion of potassium antimonide to K_2CsSb upon cesium deposition, is correlated with changes in the quantum efficiency. [http://dx.doi.org/10.1063/1.4902544]

In the last years, the electron beam physics community has identified photocathodes as a key area of research needed to meet the challenges of next generation light sources, where in particular, electron beams with very high repetition rate and low emittance will be required.[1,2] Bi-Alkali antimonide cathodes are prime candidates for next generation photoinjectors and have been the subject of intense research activity,[3–6] but much about the materials science of these systems needs to be explored before they can be adopted as robust technologies. Here, we present results from a new tool for production and analysis of accelerator photocathodes. This device permits true *in situ* x-ray studies of alkali antimonide cathodes during growth, including x-ray diffraction (XRD), x-ray reflectivity (XRR), and grazing Incidence Small Angle X-ray Scattering (GISAXS). In this paper, we present the growth dynamics of K_3Sb and K_2CsSb, and provide insight into the connection between the crystal structure, growth parameters, and the resulting Quantum Efficiency (QE).

In the presented study, *in-situ* film growth and real-time XRD measurements were performed at the X21 beamline of the National Synchrotron Light Source (NSLS) at Brookhaven National Laboratory (BNL). The experiments were performed with a photon flux of approximately $2{\cdot}10^{12}$ ph/s with an energy of 10 keV (λ = 1.2398 Å). The incident x-ray beam was 1 mm wide and 0.5 mm high. The experiment was performed using a 4 axis diffractometer with two Pilatus 100 K X-ray cameras. One of the cameras was situated in small angle scattering/reflection mode while the other simultaneously recorded wide angle diffraction data during the deposition. The first camera was at 78.5 cm from the sample and normal to the X-ray beam. The second camera was mounted at a distance of 19.7 cm from the sample and an angle of 25° vertically out of plane.

[a]Present address: Fritz Haber Institute, Faradayweg 4-6,14195 Berlin, Germany.
[b]Present address: SLAC National Accelerator Laboratory, California 94025-7015, USA.
[c]Author to whom correspondence should be addressed. Electronic mail: smedley@bnl.gov

The base pressure of the ultra-high vacuum growth chamber was 2×10^{-10} Torr throughout the experiment; a residual gas analyzer (RGA) was used to monitor contaminants during growth. Values of H_2O, CO, and CO_2 partial pressures never exceeded 2×10^{-10} Torr during deposition, and were typically $<5 \times 10^{-11}$ Torr. Substrates were electrically isolated during cathode growth and the photocurrent was monitored by applying a negative bias of about −20 V. The laser with 532 nm wavelength was positioned approximately 25 cm from the cathode surface; the diameter of the laser spot on the surface was about 1 mm. The incidence angle was 45°. The photocurrent was measured with a Keithley 6517B. Deposition rates were recorded using a quartz crystal film thickness monitor (FTM). During growth, the x-ray incidence angle onto the sample was kept at 1.8°, and the center of camera 1 was kept at 5° with respect to the beam. This geometry resulted in the beam spot overfilling the 2 cm wide substrate. After each growth step, theta-2theta scans were taken to determine the crystal texture.

We traced the process of growth of several K_2CsSb photocathodes on Si(100) using simultaneous *in-situ* XRD and QE measurements. Si(100) was chosen as substrate because it provides an atomically flat surface, enabling a precise measurement of the roughness introduction due to the material growth. Also, it has been reported that the combination of K_2CsSb grown on Si(100) was used as photocathode in a photoinjector[7] and the conductivity of the p-type Si-wafer simplifies the quantum efficiency measurement. Cathodes were grown following the recipe described by Sommer for the preparation of photomultiplier tubes (PMT),[8] where the sequence of evaporation starts with the antimony deposition onto the substrate, and subsequent alkali evaporations are performed sequentially, first potassium and then cesium. Antimony is evaporated from PtSb beads while the substrate is held at 100 °C and alkalis from Alvatec® sources while the substrate temperature is held at 135 °C. The QE at 532 nm is monitored during alkali deposition, and once a plateau is reached, the evaporation is stopped. Unlike in Sommer's studies, the cathodes were grown at lower temperatures on Si(100) substrates. The reason for this is that for cathodes that are grown on substrates that will be used in photoinjectors, the geometry must be open, to allow free access to transfer the cathode. In PMTs, the geometry is closed during manufacturing, effectively trapping the evaporated materials. The p-type Si wafer was treated with HF to remove the native oxide and rinsed with water. Even though the sample was hydrogen passivated, the brief exposure to air during mounting and transfer meant that the presence of some residual reacted oxygen cannot be excluded.

Figure 1 shows the *in-situ* diffraction results where the evolution of the crystal structure during growth for two of the fabricated cathodes is presented. Figure 1(1a) shows the evolution of the Sb structure with time at an Sb deposition rate of 0.2 A/s for a substrate at room temperature. Initially Sb grows amorphously but at a thickness of 40 Å, Bragg peaks develop over a thickness range of a few Angstrom, and the Sb is transformed into a partially textured crystalline form. We see the (012), (104), and (110) Bragg peaks with our particular detector configuration. Figure 1(2a) shows the same growth, but now for the substrate at 100 °C. We see again the same three Bragg peaks, but now with different intensities, due to the different textures of the two films. Again, the amorphous to crystalline transition occurs over a few Angstrom window at 40 Å thickness, though the process is recorded at different time scales due to different evaporation onsets. The existence of this transition has been previously reported for somewhat thicker layers, but the exact value is known to depend on substrate and deposition rate.[9,10]

Of particular interest is the observation that the onset of K deposition does not change the crystal structure. After approximately 200 Å of K is evaporated, the Sb structure fully dissolves into an amorphous phase in both cathodes; this appears to occur over the entire sample simultaneously within the 20 s time resolution of the experiment.

Further deposition of potassium results in a transition to a heterogeneous K-Sb phase by the time QE reaches a maximum value of 0.12% (0.5%) after 339 Å (232 Å) of K are deposited. Previous work found that only an ordered K_3Sb phase was formed, but we clearly see the formation of a mixed K-Sb phase after the QE reaches a maximum.[11] Subsequent θ-2θ scans after evaporation unambiguously identify these peaks as cubic K_3Sb coexisting with hexagonal K_3Sb, as well as KSb, KSb_2, K_5Sb_4, K_5Sb_4 phases.

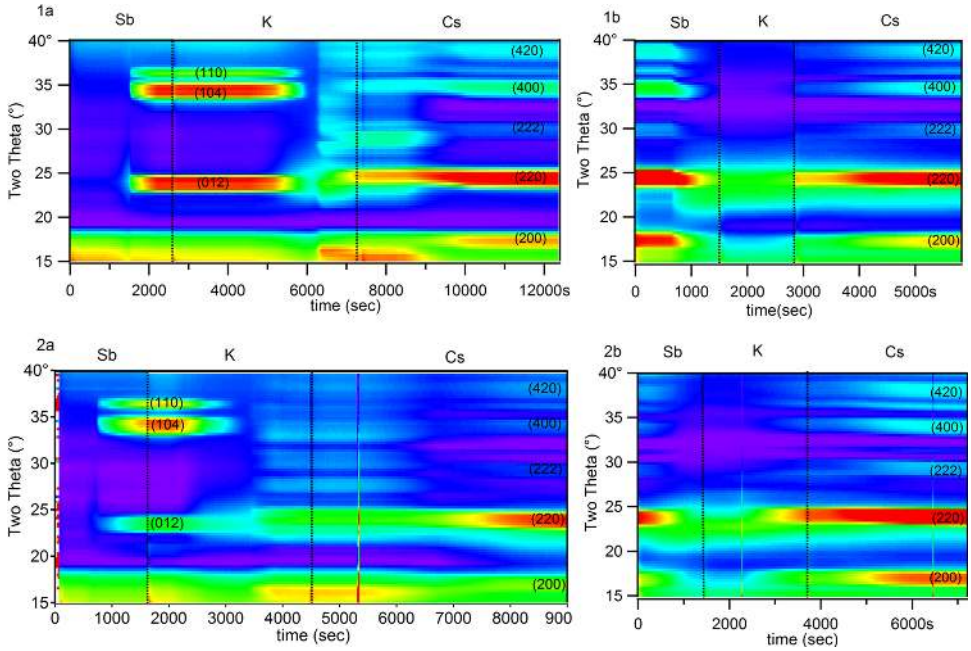

FIG. 1. *In situ* XRD measurements during growth of four K_2CsSb photocathodes. (1a) Growth on pristine Si(100) and with Sb deposition at RT. (1b) Growth on top of the previous cathode (1a). (2a) Growth on pristine Si(100) at 100 °C. (1a) Growth on top of the previous cathode (2b).

Concurrent experiments, where mainly cubic K_3Sb is obtained ,were performed by means of a process where Sb and K depositions were alternated. This PMTs processing methodology provided outstanding QE values up to 1% at 532 nm for K_3Sb. However, subsequent cesiation was unsuccessful in terms of reaching high QE values. It is evident from these results that a cubic K_3Sb phase with a predominantly (200) phase does not yield in a high QE K_2CsSb photocathodes. Further experiments are underway that aim to elucidate the correlation between cubic and hexagonal K_3Sb structures and their role in the final K_2CsSb cathode performance.[12] The general conclusion can however be drawn that a complex mixed phase K-Sb system instead of a predominantly (200) cubic phase K_3Sb is essential for the production of highly photosensitive K_2CsSb photocathodes.

Final Cs deposition provides a new crystalline structure which evolves to a final pure cubic K_2CsSb structure, with a QE performance of 1.7% (and 4%) obtained after 756 Å (and 300 Å) of Cs is evaporated over the heterogeneous K-Sb phase. This final crystalline structure is unambiguously identified as pure cubic K_2CsSb structure where five Bragg peaks are identified as (200) at 16.5°, (220) at 23.5°, (222) at 28.8°, (400) at 33.4°, and (420) at 37.5°. All K_2CsSb materials exhibiting a QE ≥ 1.5% show predominantly (220) and (222) peaks in the θ-2θ scans.

Moreover, we can infer from the XRD intensity results that the higher the contribution of the (220) and (222) phases the higher the QE. Assuming that XRD intensity is proportional to the crystalline volume,[13] we can confirm that the photocathodes with higher QE can be obtained by tuning the phases in order to increase the (220) and (222) phases. This pattern has been confirmed with up to ten cathodes with excellent QE performance (>4%).

In order to get an insight into the effect which the initial layer has on the final photoresponse and structure of the K_2CsSb photocathode, subsequent evaporations were performed on top of the existing photocathodes. Previous studies by Dowell *et al.*[14] showed that deposition of a new layer of K_2CsSb onto an already existing photocathode can enhance the QE. In our studies after depositing the first layer, the subsequent x-ray diffraction measurements usually take up to 90 min in which the QE slightly decreases. Therefore, the cathode growth was started again and the growth procedure described above was repeated. Figure 1(1b) and Figure 1(2b) show the crystalline changes in the in x,y plane x-ray diffraction during this second photocathode layer growth . In both cases, the evaporation of 165 Å of antimony is enough to remove any crystalline signature of the K_2CsSb

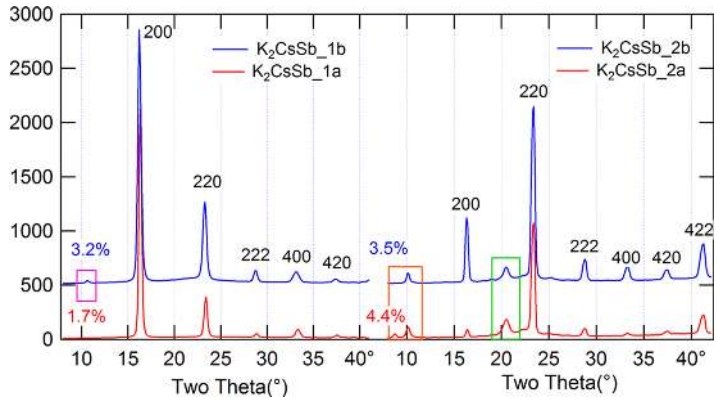

FIG. 2. Crystallographic fingerprints: θ-2θ scans after each cesium evaporation.

structure. The background of the measurement increases indicating the formation of a highly disordered phase. Then, after 275 Å and 323 Å of K are evaporated, respectively, a maximum QE value of 0.6% is obtained for both cathodes, once again heterogeneous K-Sb phases are formed. Finally, after 789 Å of Cs is evaporated in the first cathode and 630 Å in the second cathode, the crystalline fingerprint of the cubic K_2CsSb is recovered in both cases with a similar final QE of 3.2% and 3.5%, respectively.

Furthermore, θ-2θ scans after Cs evaporation were taken so crystalline fingerprints of the final K_2CsSb cathode can be compared. Figure 2 summarizes the θ-2θ scans after K_2CsSb cathode growth was completed. K_2CsSb-1a and K_2CsSb-1b correspond to the first cathode grown on top of the pristine substrate and the cathode grown on top, respectively, while K_2CsSb-2a and K_2CsSb-2b correspond to the same sequence for the second cathode layer. The immediate comparison of these scans suggests excellent crystal structures in all of them. Even though some unidentified crystalline contributions are present in some samples, it seems that they do not have a high impact on the photocathode quantum efficiency performance.

In addition to these results, complementary QE at 532 nm and thickness evolution were monitored during each of the subsequent alkali depositions. The evolution of QE correlates to the crystalline phase changes described in XRD *in-situ* measurements. Figure 3(a) shows the QE during potassium deposition. In all our measurements, a transient rise in QE occurs at 8 Å of potassium. At this point, the XRD shows only antimony structure; this rise is likely due to an alkali surface layer reducing the workfunction of the antimony metal. The QE does not change significantly during potassium deposition until the point at which K_3Sb formation is observed via XRD after 230 Å of potassium has been deposited. The maximum value of 0.12% is reached at 310 Å of potassium.

Figure 3(b) shows the QE during cesium deposition on Figure 1(1a). Unlike the potassium deposition, the QE begins to change as soon as cesitation has begun. This corresponds to the beginning of the conversion of K_3Sb into K_2CsSb, which as illustrated above is a gradual process. The dual slope observed in the area labeled II may suggest that there are different conversion rates for the two

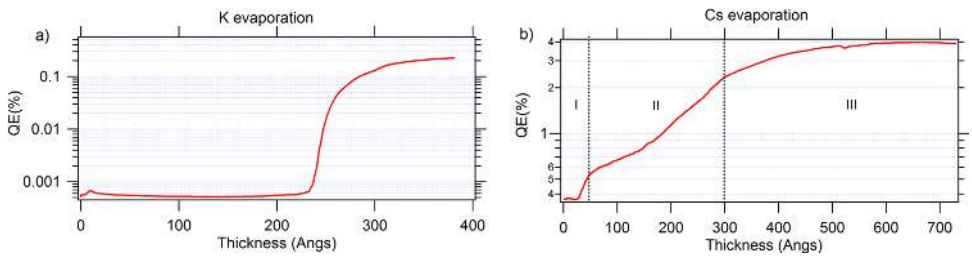

FIG. 3. QE vs thickness evolution for both of the alkali depositions. (a) QE(%) evolution during K deposition. (b) QE(%) evolution during Cs deposition for a photocathode grown at 100 °C substrate temperature.

phases of K_3Sb (cubic and hexagonal) observed in the cathode. The final QE was 4%, after 750 Å of cesium was deposited.

In conclusion, the evolution of the crystalline structure of multi-alkali photocathodes has been investigated via *in-situ* x-ray diffraction combined with photoresponse measurements which allow us to correlate structural crystalline changes with modifications in the yield. Additionally, crystallographic fingerprints by means of θ-2θ scans are reported for final steps of growth for two K_2CsSb photocathodes grown on pristine Si(100) as well as on top of the existing photocathodes.

Upon Sb evaporation, the amorphous-crystalline transition has been reported to occur within a thickness range of a few Angstroms around 40 Å for both cathodes at an evaporation rate of 0.2 Å/s and RT and 100 °C substrate, temperature, respectively. The general conclusion can be drawn that a complex mixed phase K-Sb system is essential for the production of high QE K_2CsSb photocathodes.

Finally, a crystalline fingerprint for high quality K_2CsSb photocathodes has been established, where values from 4% to 8% of QE are obtained only when crystalline phase (200) is absent and (220) is maximum.

This work was supported by the U.S. Department of Energy, under Contracts DE-AC02-05CH11231, DE-AC02-98CH10886, KC0407-ALSJNT-I0013, DE-FG02-12ER41837, and the German BMBF, Helmholtz-Association and Land Berlin.

[1] T. Rao, A. Burrill, X. Y. Chang, J. Smedley, T. Nishitani, C. Hernandez-Garcia, M. Poelker, E. Seddon, F. E. Hannon, C. K. Sinclair, J. Lewelle, and D. Feldman, "Photocathodes for the energy recovery linac," Nucl. Instrum. Methods Phys. Res., Sect. A **557**, 124–130 (2006).

[2] D. H. Dowell, I. Bazarov, B. Dunham, K. Harkay, C. Hernandez-Garcia, R. Legg, H. Padmore, T. Rao, J. Smedley, and W. Wan, "Cathode R&D for future light sources," Nucl. Instrum. Methodes Phys. Res., Sect. A **622**, 685–697 (2010).

[3] R. R. Mammei, R. Suleiman, J. Feingold, P. A. Adderley, J. Clark, S. Covert, J. Grames, J. Hansknecht, D. Machie, M. Poelker, T. Rao, J. Smedley, J. Walsh, J. L. McCarter, and M. Ruiz-Osés, "Charge lifetime measurements at high average current using a K_2CsSb photocathode inside a dc high voltage photogun," Phys. Rev. Spec. Top. - Accel. Beams **16**, 033401 (2013).

[4] S. H. Kong, J. Kinross-Wright, D. C. Nguyen, and R. L. Sheffield, "Photocathodes for free electron lasers," Nucl. Instrum. Methodes Phys. Res., Sect. A **358**(1), 272–275 (1995).

[5] T. Vecchione, I. Ben-Zvi, D. H. Dowell, J. Feng, T. Rao, J. Smedley, W. Wan, and H. A. Padmore, "A low emittance and high efficiency visible light photocathode for high brightness accelerator-based x-ray light sources," Appl. Phys. Lett. **99**, 034103 (2011).

[6] L. Cultrera, I. Bazarov, A. Bartnik, B. Dunham, S. Karkare, R. Merluzzi, and M. Nichols, "Thermal emittance and response time of a cesium antimonide photocathode," Appl. Phys. Lett. **99**(15), 152110 (2011).

[7] L. Cultrera, J. Maxson, I. Bazarov, S. Belomestnykh, J. Dobbins, B. Dunham, S. Karkare, R. Kaplan, V. Kostroun, Y. Li, X. Lui, F. Loehl, K. Smolenski, Z. Zhao, D. Rice, P. Quigley, M. Tigner, V. Veshcherevich, K. Finkelstein, D. Dale, and B. Pichler, "Photocathode behavior during high current running in the cornell energy recovery linac photoinjector," Phys. Rev. Spec. Top. - Accel. Beams **14**, 120101 (2012).

[8] A. H. Sommer, *Photoemissive Materials: Preparation , Properties and Uses* (John Wiley & Sons, Inc., 1969).

[9] A. H. Sommer, "Characteristics of evaporated antimony films as a function of the antimony source," J. Appl. Phys. **37**(7), 2789–2791 (1966).

[10] G. A. Condas, "Properties and preparation of thin antimony films of high uniformity," Rev. Sci. Instrum. **33**(9), 987–991 (1962).

[11] A. A. Dowman, T. H. Jones, and A. H. Beck, "Scanning electron diffraction studies on alkali antimonide photocathodes, including the s20," J. Phys. D: Appl. Phys. **8**, 69–84 (1975).

[12] S. Schubert, K. Attenkofer, J. Smedley, T. Kamps, M. Schmeisser, E. Muller, M. Ruiz-Osés, H. Padmore, J. Wong, and J. Xie, in *Influence of Growth Method on K_3SB Photocathode Structure and Performance* (Proceedings of IPAC14, MOPRI018, Dresden, Germany).

[13] M. Putero, B. Duployer, I. Blum, T. Ouled-Khachroum, M.-V. Coulet, C. Perrin, E. Ziegler, C. Muller, and D. Mangelinck, "Combined in situ x-ray scattering and electrical measurements for characterizing phase transformations in nanometric functional films," Thin Solid Films **541**, 21–27 (2013).

[14] D. H. Dowell, S. Z. Bethel, and K. D. Friddell, "Results from the average power laser experiment photocathode injector test," Nucl. Instrum. Methodes Phys. Res., Sect. A **356**(2), 167–176 (1995).